Local frustration determines loop opening in protein-protein association

Lukas S. Stelzl,[†,¶] Despoina A. I. Mavridou,[†,§] Andrew J. Baldwin,[‡] Stuart J. Ferguson,[†] Mark S. P. Sansom,[*,†] and Christina Redfield[*,†]

†*Department of Biochemistry, University of Oxford, South Parks Road, Oxford OX1 3QU, U.K.*

‡*Department of Chemistry, Physical and Theoretical Chemistry Laboratory, University of Oxford,Oxford OX1 3QZ, U.K.*

¶*Current address: Department of Theoretical Biophysics, Max Planck Institute of Biophysics, Max-von-Laue Str. 3, 60438 Frankfurt, Germany*

§*Current address: MRC Centre for Molecular Bacteriology and Infection, Department of Life Sciences, Imperial College London, Kensington, London, SW7 2DD, UK*

E-mail: mark.sansom@bioch.ox.ac.uk; christina.redfield@bioch.ox.ac.uk

Abstract

Local structural frustration, the existence of mutually exclusive competing interactions, may explain why some proteins are dynamic when others are rigid. More specifically, frustration is thought to play a key role in biomolecular recognition while it can also underpin the flexibility of binding sites. Here we show how a seemingly small chemical modification, the oxidation of two cysteine thiols to form a disulfide bond, during the biological function of the N-terminal domain of the bacterial oxidoreductase DsbD (nDsbD), introduces frustration. In oxidised nDsbD, local frustration disrupts the packing of the protective cap loop region against the active site of the protein allowing loop opening By contrast, in reduced nDsbD, lacking a disulfide bond, the

cap loop is rigid, always shielding the active-site cysteines and protecting them from the otherwise oxidising environment of the bacterial periplasm. Our results point towards an intricate coupling between the dynamics of the active-site cysteines and those of the cap loop, which shapes the protein-protein association reactions of nDsbD resulting in optimised protein function.

Introduction

Molecular recognition, the specific non-covalent interaction between two or more molecules, underpins all biological processes. During protein-protein association, molecular recognition often depends on conformational changes in one or both of the protein partners. Important insight into the mechansims of molecular recognition has come from NMR experiments probing dynamics at the μs-ms timescale, which often underpin protein-protein interactions.[1,2] NMR, and especially the relaxation dispersion method, is unique in being able to provide not only kinetic but also structural information about the conformational changes occuring during protein association.[3,4] In some cases, molecular dynamics (MD) simulations have been successfully paired with NMR experiments[5–8] to reveal the conformational dynamics in atomic detail.[9–11] However, we still do not have a general understanding of the molecular determinants which enable some proteins to access their bound-like conformation before encountering their binding partners in a 'conformational-selection' mechanism, while others undergo conformational change after recognising their ligands in an 'induced-fit' mechanism.[12]

Local structural frustration,[13] the existence of multiple favourable interactions which cannot be satisfied at the same time, has emerged as an important concept in rationalising why some regions in proteins undergo conformational changes in the absence of a binding partner.[14–16] Proteins are globally minimally frustrated and, thus, adopt well-defined native structures. Nonetheless, the existence of a set of competing local interactions can establish a dynamic equilibrium between distinct conformational states. Locally frustrated interac-

tions[17] are indeed more common in binding interfaces of protein complexes[14] and play an important role in determining which parts of the interacting molecules are flexible. However, relatively few studies[18,19] have analysed in atomic detail how frustration shapes conformational dynamics and, therefore, can enable protein association. This lack of understanding will hamper the exploitation of local frustration, and associated dynamic equilibria, as a design principle for synthetic molecular machines and switches.

To understand the role of frustration and dynamics we study the N-terminal domain of the transmembrane protein DsbD (nDsbD), a central oxidoreductase in the periplasm of Gram-negative bacteria. DsbD is a three-domain membrane protein (Fig. 1A) which acquires reductant from cytoplasmic thioredoxin and, through a series of thiol-disulfide exchange reactions involving pairs of cysteine residues (Fig. 1B), transfers this reductant to multiple periplasmic pathways (Fig. 1A).[20,21] nDsbD plays a critical role as the hub for reductant provision in the bacterial periplasm.[22] It interacts with the C-terminal domain of DsbD (cDsbD) to acquire the reductant provided by cytoplasmic thioredoxin and then also interacts with several globular periplasmic partners, including DsbC, CcmG and DsbG, to provide reductant (Fig. 1A). All these reductant exchange steps involve close interactions between nDsbD and its binding partners, which are essential so that their functional cysteine pairs can come into proximity leading to reductant transfer.[23,24]

X-ray structures show that the cap-loop region of nDsbD, containing residues D68-E69-F70-Y71-G72, plays a key role in the association reactions of nDsbD with its binding partners.[23,25,26] The catalytic subdomain of nDsbD is inserted in the antigen-binding end of its immunoglobulin (Ig) fold with the two active-site cysteines, C103 and C109, located on opposite strands of a β-hairpin (Fig. 1C). For both oxidation states of isolated nDsbD (with and without a disulfide bond between C103 and C109), the active-site cysteines are shielded by the cap-loop region which adopts a closed conformation.[23,24,27,28] Strikingly, all structures of nDsbD in complex with its binding partners, cDsbD, DsbC, and CcmG,[23,25,26] show the cap loop in an open conformation allowing interaction of the cysteine pairs of the two proteins

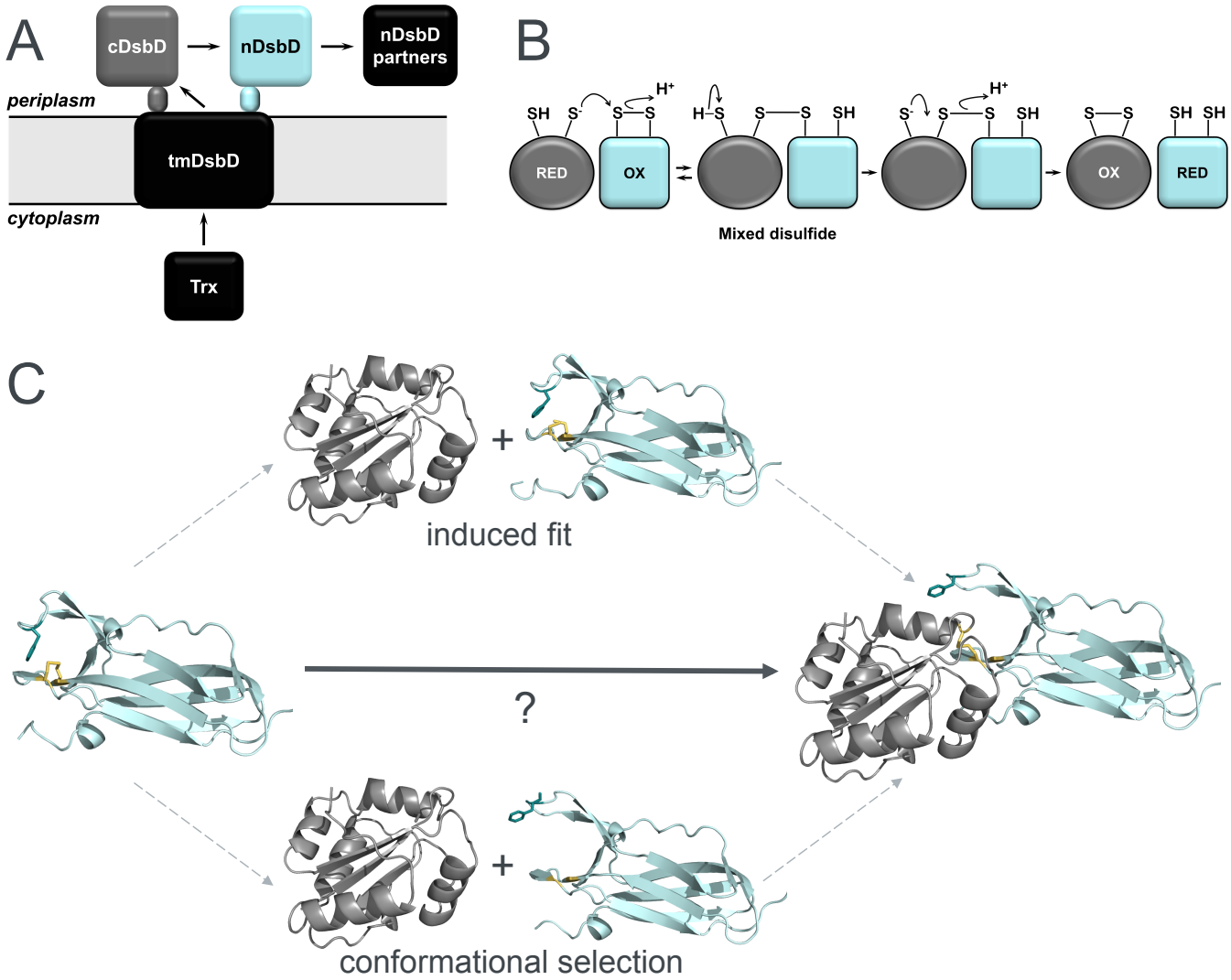

Figure 1: Function of nDsbD and the opening mechanism of the cap loop. (A) The oxidoreductase DsbD has three domains, a central domain with transmembrane helixes (tmDsbD), and two periplasmic globular domains (nDsbD and cDsbD). The pathway of reductant flow from thioredoxin (Trx) in the cytoplasm, via the three domains of DsbD to the other periplasmic pathways is shown. Trx_{red} reduces the disulfide bond in $tmDsbD_{ox}$, $tmDsbD_{red}$ then reduces $cDsbD_{ox}$, and $cDsbD_{red}$ then reduces $nDsbD_{ox}$. DsbC, CcmG and DsbG then accept reductant from $nDsbD_{red}$. (B) Schematic representation of the thiol:disulfide exchange reaction (bimolecular nucleophilic substitution mechanism) between cDsbD and nDsbD. (C) Oxidised nDsbD, which adopts an immunoglobulin fold, is illustrated on the left in cyan (PDB: 1L6P). The cap loop (residues 68-72) which covers the active site is highlighted in teal. The side chain of F70 (shown in a surface representation) shields the active-site disulfide bond (between C103 and C109, shown in yellow) in the closed cap-loop conformation. The cap loop of nDsbD adopts an open conformation in the covalent mixed-disulfide complex of nDsbD and cDsbD (PDB: 1VRS) shown on the right. This allows the interaction of the cysteine residues of the two domains. cDsbD, shown in grey, has the thioredoxin fold typical of oxidoreductases. The central panels illustrate two possible mechanisms by which cap loop opening might occur to allow the formation of the nDsbD-cDsbD complex.

(Fig. 1C).[23,26,29]

While these structures provide static snapshots of the closed and open states of the cap loop, they do not provide any insight into the mechanism of loop opening that is essential for the function of nDsbD. To understand the drivers of this conformational change, two hypotheses regarding the solution state of nDsbD need to be examined (Fig. 1C). (1) It is possible that the cap loop only opens when nDsbD encounters its binding partners, an 'induced-fit' mechanism consistent with the hypothesised protective role of this region of the protein.[27] (2) It is also plausible that in solution the cap loop is flexible so that it samples open states allowing binding of partner proteins via 'conformational selection'.[12] Of course, if the cap loop does open in the absence of a binding partner, that could compromise the transfer of reductant in an oxidising environment like the periplasm. Therefore, a protective role for the cap loop could be more important in reduced nDsbD ($nDsbD_{red}$), so the possibility that nDsbD interacts with its partners via different loop-opening mechanisms depending on its oxidation state also needs to be considered. In this scenario, the pair of cysteine could modulate the conformational ensemble of nDsbD as has been hinted at by structural bioinformatics.[30,31]

Here we use both NMR experiments and MD simulations to describe different behaviours for the cap loop depending on the oxidation state of nDsbD. The atomic-scale insight afforded by these two methods reveals how the disulfide bond introduces local frustration specifically in oxidised nDsbD ($nDsbD_{ox}$), allowing the cap loop and active site in $nDsbD_{ox}$ to sample bound-like conformations in the absence of a binding partner. Our observations have implications not only for the function of DsbD, but more broadly for the role of local frustration in ensuring optimised protein-protein interactions.

Materials and Methods

Construction of plasmids

Plasmids used in this study are listed in Table S1. The plasmid pDzn3, described in previous work,[32,33] encodes isolated wild-type (WT) nDsbD (L2-V132) bearing a thrombin-cleavable C-terminal polyhistidine tag. This construct was used as a template to produce a cap-loop deletion variant of nDsbD (Δloop-nDsbD), where residues H66-K73 were replaced by the amino acid sequence A-G-G. Site-directed mutagenesis (QuikChange, Qiagen) was performed using oligonucleotides 5'-(AGGAAGCGAGATTTACCGCGATCGGCTG)-3' and 5'-(CCGGCCCAGACGC CTTGCGGCAGCTGC)-3'; the resulting plasmid was named pDzn8. DNA manipulations were conducted using standard methods. PCR was performed with KOD Hot Start DNA polymerase (Novagen) and oligonucleotides were synthesized by Sigma Aldrich.

Protein production, purification and characterization

Isolated WT nDsbD and Δloop-nDsbD were expressed using BL21(DE3) cells (Stratagene) and were purified from periplasmic extracts of *E. coli* using a C-terminal polyhistidine tag. Thrombin cleavage of the affinity tag was performed using the Sigma Thrombin CleanCleave Kit (Sigma) according to the manufacturer's instructions. Production and purification of all protein samples was carried out as described previously.[32,34]

NMR spectroscopy

NMR experiments were conducted using home-built 500, 600 and 750 MHz spectrometers equipped with Oxford Instruments Company magnets, home-built triple-resonance pulsed-field gradient probeheads and GE/Omega data acquisition computers and software. All experiments were conducted at 25 °C and at pH 6.5 in 95% H_2O/5% D_2O, unless stated otherwise. Spectra were processed using NMRPipe[35] and analysed using CCPN Analysis.[36,37]

Residual dipolar couplings (RDCs) were measured using Pf1 phage purchased from ASLA BIOTECH Ltd. (Riga, Latvia). RDCs were measured at 600 MHz for 0.5 mM nDsbD with 10 mg/ml Pf1 phage, 2 mM K_2PO_4, 0.4 mM $MgCl_2$, 0.01 % NaN_3 and 10 % D_2O. Measurements were carried out for isotropic solutions prior to the addition of the Pf1 phage. Separate samples were used for oxidised and reduced nDsbD. RDCs were measured using the InPhase-AntiPhase (IPAP) approach.[38] The F_2 (^{1}H) and F_1 (^{15}N) dimensions were recorded with sweep widths of 7518.8 and 2000.0 Hz, respectively, and with 1024 and 128 complex points, respectively, with 128 scans per increment. The quality factor (Q) that describes the agreement between calculated and observed RDCs was determined using the procedure of Ottiger et al.[39]

{^{1}H}-^{15}N heteronuclear NOE, ^{15}N T_1 and T_2 data[40–42] were measured at 600 MHz. The {^{1}H}-^{15}N heteronuclear NOE was also measured at 500 MHz. For the T_1 measurement, spectra with 14 different relaxation delays, ranging from 20 ms to 2 s, were collected. The T_2 was measured by recording spectra with 14 relaxation delays, between 8 ms and 400 ms, with a Carr-Purcell Meiboom Gill (CPMG) delay (τ_{CPMG}) of 0.5 ms. In the T_1 and T_2 measurements, a recycle delay of 2 s was used. The {^{1}H}-^{15}N NOE was measured by comparing peak heights in interleaved spectra recorded with and without saturation of the protons for 3 and 4 s at 500 and 600 MHz, respectively. The F_2 (^{1}H) and F_1 (^{15}N) dimensions were recorded with sweep widths of 7518.8 and 1785.7 Hz, respectively, and with 1024 and 128 complex points, respectively. The T_1, T_2 and NOE experiments were collected with 16, 16 and 128 scans per increment.

^{15}N relaxation data were collected for 107 and 117 of the 126 non-proline residues of oxidised and reduced nDsbD, respectively. Data for the remaining residues could not be measured due to weak or overlapping peaks. T_1, T_2 and the {^{1}H}-^{15}N NOE values and associated errors were determined as described in detail previously.[43] Relaxation data were analyzed using in-house software;[43] this incorporates the model-free formalism of Lipari and Szabo,[44,45] using spectral density functions appropriate for axially-symmetric rotational

diffusion[46] and non-colinearity of the N-H bond vector and the principal component of the ^{15}N chemical shift tensor,[47] with model selection and Monte Carlo error estimation as described by Mandel et al.[48] Calculations were carried out using an N-H bond length of 1.02 Å, a ^{15}N chemical shift anisotropy, $(\sigma_{\parallel} - \sigma_{\perp})$, of -160 ppm, and a $D_{\parallel}/D_{\perp}$ ratio of 2.0.

^{15}N relaxation-dispersion experiments[49] were recorded at multiple magnetic field strengths and temperatures. Recycle delays of 1.2 and 1.5 s were used at 500 and 750 MHz, respectively. Typically 12 to 14 spectra were recorded with refocusing fields, ν_{CPMG}, between 50 and 850 Hz and two reference spectra[50] were collected to convert measured peak intensities into relaxation rates. At 15 °C and 25 °C, experiments were collected at both 500 and 750 MHz. Experiments at 10 °C, 20 °C and 35 °C were recorded at 500 MHz only. The cap-loop deletion mutant, Δloop-nDsbD, was studied at 25 °C at 750 MHz. The experiments were analysed by global fitting using CATIA (Cpmg, Anti-trosy, and Trosy Intelligent Analysis, http://www.biochem.ucl.ac.uk/hansen/catia/)[51–53] using transition state theory to restrict the rates and linear temperature-dependent changes in chemical shifts when analysing data across multiple temperatures.[52,53]

The HSQC and HMQC pulse sequences developed by Skrynnikov et al.[54] were used to determine the sign of the chemical shift differences between the major and minor states. Experiments were recorded at 750 MHz with 64 scans per increment, ^{1}H and ^{15}N sweep widths of 9433.96 and 2304.15 Hz, respectively, and with 1024 and 128 complex points in the ^{1}H and ^{15}N dimensions, respectively.

Molecular dynamics simulations

MD simulations were run using GROMACS 4.5.[55] Simulations were started from the closed crystal structures of reduced nDsbD ($\mathrm{nDsbD_{red}}$) (PDB: 3PFU)[24] and oxidised nDsbD ($\mathrm{nDsbD_{ox}}$) (PDB 1L6P).[27] For each redox state of nDsbD, four simulations of 200 ns and ten simulations of 20 ns, all with different initial velocities, were run giving a combined duration of 1 μs for each protein. Trajectories were also initiated from open structures (PDB: 1VRS chain B);[25]

eight and ten 10 ns trajectories were run for $nDsbD_{red}$ and $nDsbD_{ox}$, respectively. Missing side-chain atoms were added using the WHAT-IF Server.[56] The histidine side chains were protonated and the cysteine side chains (C103 and C109) in the active site of $nDsbD_{red}$ were represented as thiols; these choices were based on pH titrations monitored by NMR.[32] The protein was embedded in rhombic dodecahedral boxes, with a minimum distance to the box edges of 12 Å at NaCl concentrations of 0.1 M. Trajectories using a larger distance of 15 Å to the box edges showed no significant differences. The CHARMM 22 force field[57] with the CMAP correction[58] and the CHARMM TIP3P water model was used. Electrostatic interactions were calculated with the Particle Mesh Ewald method (PME).[59] The Lennard-Jones potential was switched to zero, between 10 Å and 12 Å.[60] The length of bonds involving hydrogen atoms was constrained, using the PLINCs algorithm.[61] The equations of motion were integrated with a 2 fs time step. The simulation systems were relaxed by energy minimisation and 4 ns of position-restrained MD in the NVT ensemble before starting the production simulations in the NPT ensemble at 25 °C and 1 bar for 10 ns, 20 ns or 200 ns. The Bussi-Donadio-Parinello thermostat,[62] with a τ_T of 0.1 ps and the Parinello-Rahman barostat[63] with a τ_P of 0.5 ps and a compressibility of $4.5 \times 10^5\,\mathrm{bar}^{-1}$ were used.

Analysis of the MD simulations

To validate our MD simulations, amide order parameters (S^2) and residual dipolar couplings (RDCs) were calculated from them. Before calculating S^2 and RDCs we removed the overall tumbling from the simulations by aligning each frame to a reference structure. Order parameters were calculated in 5 ns blocks from the MD trajectories[64] with S^2 given by

$$S^2 = \frac{1}{2}[3\sum_{\alpha=1}^{3}\sum_{\beta=1}^{3}\langle\hat{\mu}_\alpha\hat{\mu}_\beta\rangle - 1], \tag{1}$$

where α and β denote the x,y,z components of the bond vector $\hat{\mu}$.

To calculate RDCs, the principle axes of the reference structure were aligned with the

experimentally determined alignment tensor. The use of a single reference structure is justified given the stability of the overall fold of nDsbD in the simulations. The RDC for a given residue in a given structure is then calculated using

$$\overline{D} = \frac{\kappa}{R^3}(A_x \cos^2\theta_1 + A_y \cos^2\theta_2 + A_z \cos^2\theta_3) \tag{2}$$

where κ depends on the gyromagnetic ratios $\gamma_I\gamma_S$, the magnetic permittivity of vacuum μ_0 and Planck's constant $\hbar$ and is defined as $\kappa = -\frac{3}{8\pi^2}\gamma_I\gamma_S\mu_0\hbar$. R is the bond length and is uniformly set to 1.04 Å. The angles θ_1, θ_2 and θ_3 describe the orientation of the individual bonds with respect to the three principal axes of the alignment tensor. A_x, A_y and A_z are the principal components of the alignment tensor.

Results and Discussion

The solution structure of nDsbD as probed by NMR

NMR experiments demonstrate that the cap loop has an important protective role in shielding the active-site cysteines of nDsbD. For nDsbD_{ox}, we showed previously that reduction of the disulfide bond by dithiothreitol (DTT) is very slow, indicating that the cap loop shields C103 and C109 from the reducing agent.[24] NMR spectra for $\text{nDsbD}_{\text{red}}$ collected between pH 6 and 11 show no change in cysteine C_β chemical shifts. This indicates that the pK_a of C109, the cysteine residue thought to initiate reductant transfer,[25] is above 11, thus making it unreactive in isolated $\text{nDsbD}_{\text{red}}$. The shielding of the active site by the cap loop in $\text{nDsbD}_{\text{red}}$ protects C103 and C109 from non-cognate reactions in the oxidising environment of the periplasm.

The cap loop shields the active site by adopting a closed conformation as in the X-ray structures of oxidised (PDB: 1L6P and 1JPE)[23,27] and reduced (PDB: 3PFU)[24] nDsbD. These structures are very similar to each other with pairwise C_α RMSDs for residues 12 to

122 of less than 0.15 Å. To probe the solution structure of oxidised and reduced nDsbD, we measured ^{1}H-^{15}N residual dipolar couplings (RDCs), which are sensitive reporters of protein structure (Fig. S1 and Table S2). Analysis of these data indicates that the orientation of the active-site/cap-loop residues relative to the core β-sandwich of both oxidised and reduced nDsbD in solution is well-described by the X-ray structures in which the cap loop adopts a closed conformation. Nevertheless, the cap loop must open to expose the active site in order for nDsbD to carry out its biological function.

NMR spin-relaxation experiments and model-free analysis

To investigate whether the cap loop is flexible in solution, opening and closing frequently, and whether the dynamic behaviour of the loop differs in the two oxidation states, we studied the fast time-scale (ps-ns) dynamics of nDsbD using NMR relaxation experiments. ^{15}N relaxation experiments, analysed using the "model-free" approach,[44,45] showed that most of the protein backbone is relatively rigid. The majority of order parameters (S^2) for the backbone amide bonds are above 0.8 (Fig. 2). The N- and C-terminal regions of nDsbD gave very low S^2 values and are clearly disordered in solution. Other residues with order parameters below 0.75 are located in loops and at the start or end of elements of secondary structure but are not found to be clustered in a specific region. For example, lower order parameters are observed for residues 57 and 58 in both redox states. These residues are located in a long 'loop' parallel to the core β-sandwich but not identified as a β-strand due to the absence of hydrogen bonds.

In both oxidation states, the S^2 values for the cap-loop region are similar to the rest of the folded protein. Thus, on average, the cap loop of nDsbD does not undergo large amplitude motions on a fast timescale and the active-site cysteines will remain shielded by the cap loop. However, close inspection of the $\{^{1}\text{H}\}$-^{15}N NOE values for the cap-loop residues in oxidised and reduced nDsbD does show a clear difference between the two oxidation states (Figure S2 and Table S3). In nDsbD$_{\text{ox}}$, seven residues between V64 and G72 have NOE

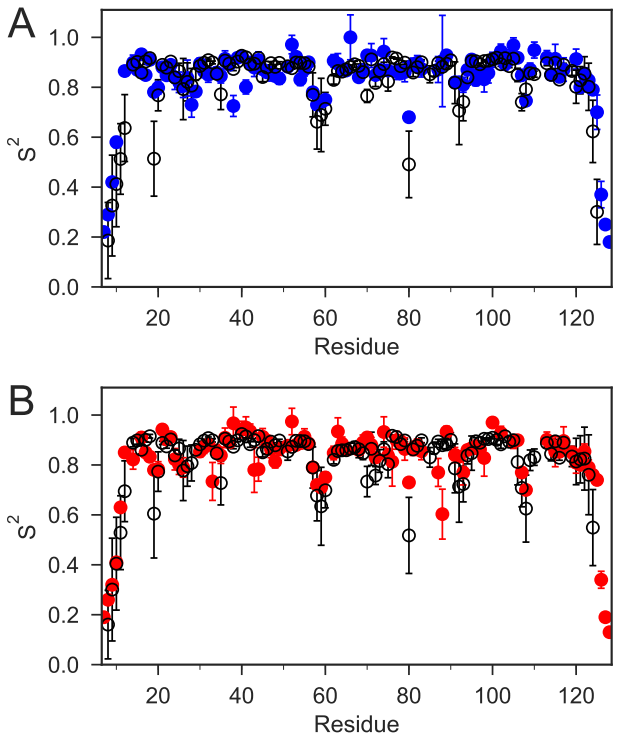

Figure 2: The order parameters (S^2) for backbone amides derived from ^{15}N relaxation experiments and MD simulations are plotted as a function of sequence. The experimental order parameters for reduced and oxidised nDsbD are shown in blue (A) and red (B), respectively. The average order parameters calculated from the combined 1 μs MD simulation ensembles starting from closed structures for reduced (A) and oxidised (B) nDsbD are shown in black. Errors in S^2 were determined by Monte Carlo simulations (experiment) and a bootstrap analysis (MD simulations). The simulations of both oxidised and reduced nDsbD reproduced even subtle features of sequence-dependent variation of S^2 values. For example, S^2 values for residues 57-60 were lowered in both experiment and simulation. These residues are not part of the regular secondary structure of the immunoglobulin fold in the both the X-ray structures of nDsbD and in the MD simulations.

values at or below 0.7 while in $nDsbD_{red}$ there is only one residue with an NOE value below 0.7. The consequence of this difference is that the majority of residues in this region in $nDsbD_{ox}$ require a more complex model (with the τ_e parameter ranging from $\sim$ 50 to 350 ps) to obtain a satisfactory fit in the analysis while the majority of residues in $nDsbD_{red}$ can be fitted with the simpler S^2-only model which assumes a τ_e value of faster than $\sim$ 10 ps. Therefore, although the amplitude of motions of cap-loop residues is limited and does not appear to differ very much between the two oxidation states, the timescale of the fast dynamics, as described by the approach of Lipari & Szabo, does differ.

Molecular dynamics simulations

To understand the differences between reduced and oxidised nDsbD and their conformational dynamics at atomic resolution, molecular dynamics (MD) simulations were employed. To track the orientation of the cap loop relative to the active site in the MD trajectories, the distance between the centre of the aromatic ring of F70 and the sulfur atom of C109 was calculated. Multiple simulations, for a total of 1 μs, were started from the X-ray structure of reduced nDsbD (3PFU). The distance between F70 and C109 remained close to the value in the X-ray structure of $nDsbD_{red}$, as shown for example trajectories in Fig. 3A and B. Opening of the cap loop in $nDsbD_{red}$ was not observed in 1 μs of simulation time (Fig. 3D). This confirms that the cap loop protects the active-site cysteines of $nDsbD_{red}$ from the oxidising environment of the periplasm

By contrast, $nDsbD_{ox}$ showed more complex dynamics in the 1 μs of simulations launched from the closed 1L6P X-ray structure. In several simulations the cap loop remained closed (Fig. 3E), only showing occasional fluctuations. In one simulation the fluctuations in the cap loop were much more pronounced (Fig. 3F). After 80 ns the cap loop opened, as judged by the F70-C109 distance, and stayed open for the remainder of the 200 ns MD trajectory. The spontaneous loop opening of $nDsbD_{ox}$ and the relative stability of partially open conformations observed in our MD simulations (Fig. 3H) marks a clear difference between the

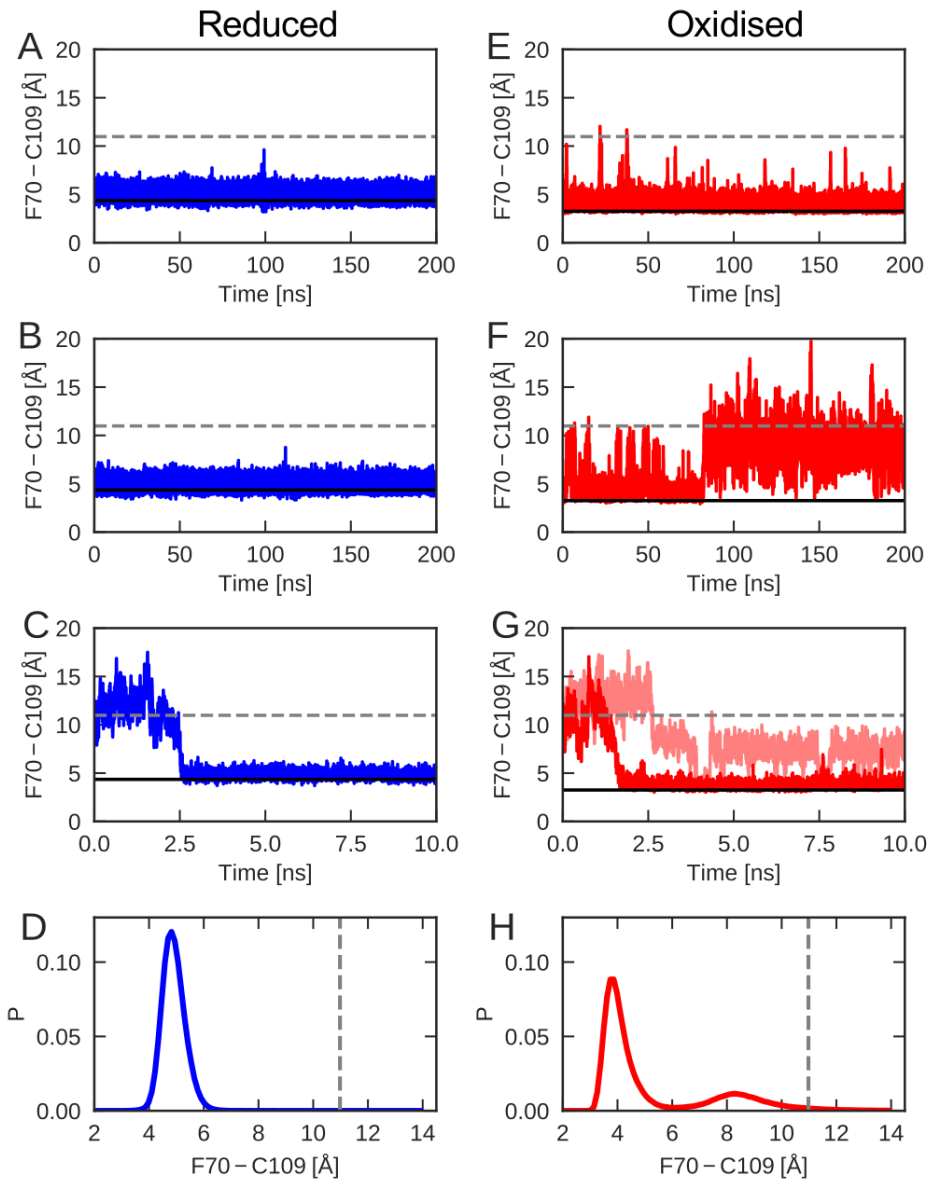

Figure 3: The cap-loop conformation has been probed in MD simulations with reduced (A-C) and oxidised (E-G) nDsbD. The conformational state of the cap loop was followed by tracking the distance between the centre of the aromatic ring of F70 and the sulfur atom of C109. The solid and dashed lines at $\sim$ 3-4 and $\sim$ 11 Å show the F70 ring to C109 Sγ distance in the closed (3PFU/1L6P) and open (1VRS) X-ray structures, respectively. The cap loop remains stably closed in simulations of nDsbD$_{red}$, as shown in (A) and (B). The cap loop in nDsbD$_{red}$ closes within 3 ns for a simulation started from an open conformation based on the 1VRS structure (C). The 1 μs simulation ensemble for nDsbD$_{red}$ shows a closed conformation of F70 relative to C109 (D). The cap loop conformation is more flexible in simulations of nDsbD$_{ox}$; in some simulations it remains closed (E) while in others the loop opens (F). The loop generally closes in simulations of nDsbD$_{ox}$ started from an open conformation (G). Overall, the 1 μs simulation ensemble for nDsbD$_{ox}$ shows a preference for the closed conformation of F70 relative to C109 with open conformations sampled relatively rarely (H)

conformational ensembles sampled by oxidised and reduced nDsbD (Fig 3D,H).

We have also employed MD to probe the behaviour of the cap loop in simulations starting from an open conformation of nDsbD observed in the 1VRS X-ray structure of the nDsbD/cDsbD complex.[25] Five of eight trajectories for $nDsbD_{red}$ started with an open loop conformation closed within 10 ns (Fig. 3C). Simulations of $nDsbD_{ox}$, started from a fully open 1VRS oxidised structure, closed within 10 ns in three out of ten trajectories (Fig. 3G). These simulations demonstrate that in both reduced and oxidised nDsbD the cap loop can close rapidly in the absence of a bound interaction partner.

To validate the MD simulations we used the trajectories to predict ^{1}H-^{15}N RDC and S^2 values and to compare these to our experimental values. RDCs provide information about the average orientation of peptide bonds and are therefore well-suited for comparison with MD simulations. For both $nDsbD_{red}$ and $nDsbD_{ox}$, the agreement between calculated and experimental RDCs improved for the 1 μs MD ensemble compared to the static X-ray structures (Fig. S1 and Table S2). The extent of the fast-time scale (ps-ns) dynamics observed experimentally by NMR is on the whole correctly reproduced by the MD simulations (Fig. 2 and S3). The trend for the cap loop is consistent with experiment, the S^2 values for the cap-loop region for both oxidised and reduced nDsbD are on par with the rest of the well-ordered protein core (Fig. S2 and Table S3). The observed cap-loop opening in the MD simulations of $nDsbD_{ox}$ is too rare an event to lower S^2 values in a significant way. However, the lowered experimental $\{^{1}H\}$-^{15}N NOE values for $nDsbD_{ox}$, and the need to fit using a model including a τ_e parameter, are consistent with the observation of loop opening events in the MD simulations for $nDsbD_{ox}$. The good level of agreement between experimental NMR parameters and values calculated from the MD trajectories provides confidence that the 1 μs simulations of oxidised and reduced nDsbD yield a realistic picture of the fast timescale dynamics of nDsbD at the atomic level.

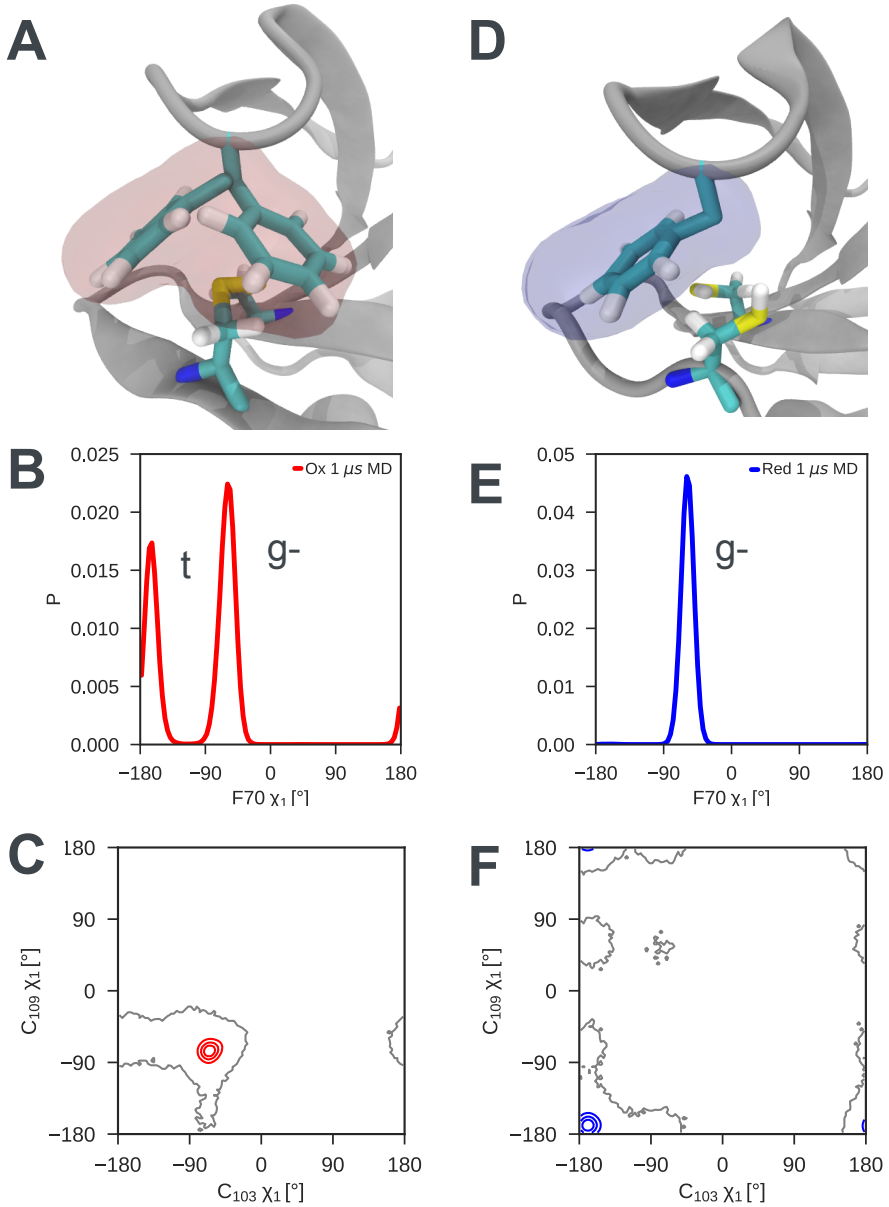

Figure 4: Local frustration destabilises the cap loop of oxidised nDsbD while the cap loop of reduced nDsbD packs stably onto the active site. In $nDsbD_{ox}$ (A), the side chain of F70 switches between a gauche- and trans orientation in MD simulations as the mass density calculated for F70 (red) shows. The surface surround points with at least 0.12 relative occupancy. The gauche- and trans conformations are approximately equally populated in the 1μs MD simulations of $nDsbD_{ox}$ (B). The cap loop and the active site of $nDsbD_{red}$ are rigid (D) as the mass density calculated for F70 (blue) shows. The well-defined density closely circumscribes the position of the F70 side chain in the 3PFU crystal structure and F70 is locked in the gauche- conformation (E). The side chains of C103 and C109 in the active site of nDsbD adopt different conformations in the oxidised (C) and reduced (F) isoforms as shown by contour plots of their χ_1 dihedral angles. Here 1 μs of MD simulations are analysed for each redox state.

NMR and MD simulations reveal local frustration in $nDsbD_{ox}$

The differences in the cap loop dynamics, with the loop being more flexible in $nDsbD_{ox}$ than in $nDsbD_{red}$, must be a direct effect of the oxidation state of the two cysteine residues in the active site of nDsbD. X-ray crystallography[24] and solution NMR show that the average structures in the two redox states are very similar. The only major difference between the two states is the presence of a disulfide bond in the active site of $nDsbD_{ox}$ and a pair of thiol groups in $nDsbD_{red}$.

Indeed, the disulfide bond introduces local structural frustration in $nDsbD_{ox}$, as F70 in the cap loop can adopt two mutually exclusive conformations and this leads to occasional cap loop opening. The side chains of C103 and C103, forming the disulfide bond, adopt gauche-conformations in X-ray structures. This conformation is maintained throughout the MD simulations with only rare excursions (Fig. 4C). The C103-C109 disulfide bond in $nDsbD_{ox}$ provides a flat binding surface for the phenyl ring of F70. As a consequence, the aromatic ring of F70 packs on to the disulfide bond with the F70 sidechain in either a gauche- or a trans orientation (Fig. 4A and B). The two orientations are populated approximately equally and exchange rapidly in MD, on a timescale of tens of ns. Since F70 is not locked in place, the cap loop is flexible and can open, as we observed in one of the MD trajectories started with closed cap loop (Fig. 3F). The conformational averaging is evidenced by the almost identical F70 Hβ chemical shifts, which differ by only 0.015 ppm. TALOS-N[65] analysis of $nDsbD_{ox}$ chemical shifts does not predict a single fixed χ_1 value for F70 consistent with the averaging between a gauche- and a trans orientation seen for this side chain in MD simulations.

By contrast, in $nDsbD_{red}$ F70 packs on to the active site in a single well-defined conformation, explaining why the cap loop is rigid in $nDsbD_{red}$. The side chains of C103 and C109 both adopt a trans conformation ($\chi_1 \approx 180°$) in the X-ray structure of $nDsbD_{red}$. This conformation is maintained throughout the MD simulations of $nDsbD_{red}$ with only rare excursions (Fig. 4F). In $nDsbD_{red}$, with the cysteines in the trans conformation and with the two cysteine thiols also bulkier than a disulfide bond, the cysteine thiols provide

a snug-fitting binding site for F70 (Fig. 4D). In addition, one of the C019 Hβ hydrogens interacts closely with the aromatic ring of F70 and this interaction could be considered a C-H π hydrogen bond.[66] Consequently, F70 is locked in its gauche- conformation (Fig. 4E).

NMR data support this packing arrangement of the cap loop onto the active site of nDsbD$_{red}$. The Hβ of C109 are upfield shifted at 1.83 and 0.66 ppm, from a random coil value of $\sim$ 3 ppm, consistent with the close proximity to the ring of F70. The two distinct Hβ shifts for F70 of nDsbD$_{red}$, which are separated by $\sim$ 0.2 ppm, show NOEs of differing intensity from the backbone H^N, consistent with a single conformation for the F70 side chain. TALOS-N[65] analysis of chemical shifts predicts a gauche- χ_1 conformation for F70, in agreement with the MD simulations.

NMR relaxation dispersion experiments

Using ^{15}N NMR relaxation dispersion experiments[1,49] we also detected a difference in the μs-ms timescale dynamics of reduced and oxidised nDsbD. For nDsbD$_{red}$, no evidence for μs-ms dynamics in the cap loop (Fig. 5A-C) or the active site were found. This observation is consistent with the absence of a significantly populated open state of nDsbD$_{red}$. By contrast, in nDsbD$_{ox}$, eight residues, V64, W65, E69, F70, Y71, G72, K73 and S74, all in the cap-loop region, showed strong relaxation dispersion effects (Fig. 5D-F and 6A). Previously, NMR relaxation-dispersion experiments and MD simulations have detected complex dynamics in BPTI stemming from one of its disulfide bonds.[67–69] This further suggests that the disulfide bond shapes the dynamics of nDsbD$_{ox}$.

The relaxation dispersion results are consistent with previous observations about peak intensities in ^{1}H-^{15}N HSQC spectra of nDsbD.[32] nDsbD$_{ox}$ shows line broadening not observed for nDsbD$_{red}$. The ^{1}H-^{15}N peaks of C103 and C109 of oxidised nDsbD, but not reduced nDsbD, are invisible,[32] likely due to extensive chemical exchange processes on the μs-ms time scale in nDsbD$_{ox}$. Similarly, A104 in the active site gives rise to only a very weak peak in the HSQC spectrum of nDsbD$_{ox}$, but a strong peak in the reduced protein. Thus the

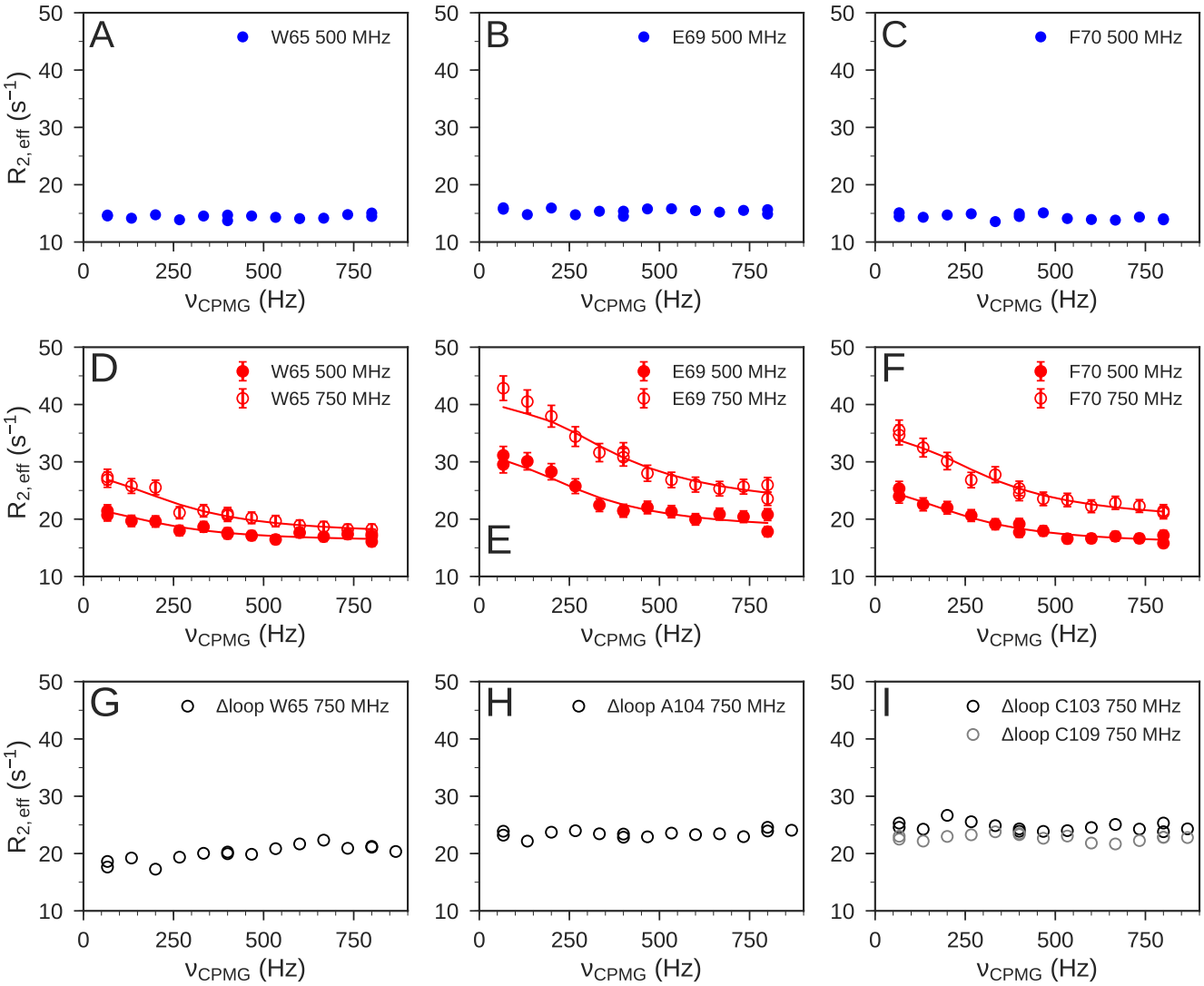

Figure 5: ^{15}N relaxation dispersion experiments were used to determine the μs-ms dynamics of nDsbD. For reduced nDsbD, flat relaxation dispersion profiles were obtained as illustrated for (A) W65, (B) E69 and (C) F70 in the cap loop. For oxidised nDsbD clear relaxation dispersion effects were measured for (D) W65, (E) E69 and (F) F70. In the oxidised cap-loop deletion mutant (Δloop-nDsbD), flat relaxation dispersion profiles were obtained are for (G) W65, and for (H) A104 and (I) C103/C109 in the active site. Experimental data are represented by circles and fits to the data for WT nDsbD$_{ox}$ are shown by solid lines.

cap loop of $nDsbD_{ox}$, and likely also the active-site cysteines of $nDsbD_{ox}$, exchange between different conformations on the μs-ms timescale, whereas the reduced protein adopts a single conformation on this timescale.

Analysing the relaxation dispersion data collected at 25 °C (using CATIA[51–53]) showed that $nDsbD_{ox}$ undergoes a single global exchange process, between a dominant major state (p_A 98 %) and an alternative minor state (p_B 2 %). To corroborate that a single exchange process gives rise to the relaxation dispersion curves, we repeated the experiments at four additional temperatures (10, 15, 20 and 35 °C). If the residues undergo different exchange processes we would expect them to show a differential response to temperature.[67] The relaxation dispersion data for all residues in the cap loop recorded at the five temperatures could be fitted simultaneously[52,53] (Figure S4A), which confirmed that a single process underlies the μs-ms chemical exchange in the cap loop of $nDsbD_{ox}$. In addition, the analysis of the data at the five temperatures yielded a detailed description of the thermodynamics and kinetics of the exchange process (Fig. S4B). The minor "excited" state is enthalpically but not entropically more favourable than the major ground state of $nDsbD_{ox}$. The fits also demonstrated that no enthalphic barrier separates the ground and excited state of $nDsbD_{ox}$. The absence of an enthalpic barrier between the two states might mean that no favourable interactions have to be broken in the transition state, but that the diffusion process itself may limit the speed of the transition.[70]

Analysis of the chemical shift differences determined from the relaxation dispersion experiments suggests that the conformation adopted by the cap loop in the minor state of $nDsbD_{ox}$ might be similar to the conformation of $nDsbD_{red}$. To interpret the chemical shift differences we calculated the shift changes expected if the minor state features a disordered cap loop. A disordered state would include more open conformations and such structures might facilitate the binding of the interaction partners of nDsbD. The lack of correlation in Fig. 6B demonstrates that the cap loop does not become disordered in the less populated minor state. The ^{15}N chemical shift differences between the major and minor states do,

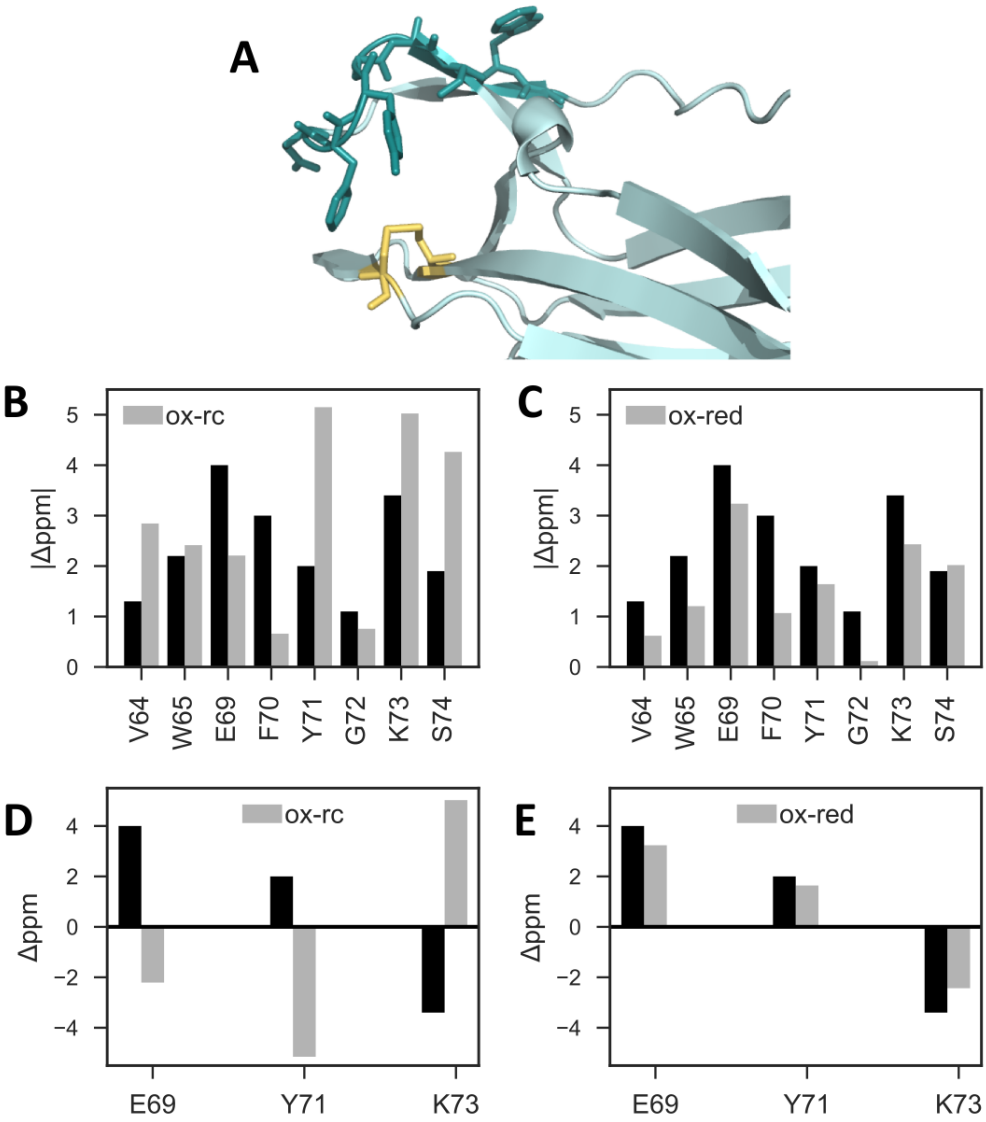

Figure 6: Structural characterisation of μs-ms dynamics in oxidised nDsbD. (A) Residues V64, W65, E69, F70, Y71, S72, K73 and S74 with chemical shift differences between the major and minor states of > 1 ppm are shown in a stick representation in dark teal. C103 and C109 are shown in yellow. The magnitude of the ^{15}N chemical shift differences between the major and minor states are compared in (B) with the magnitude of predicted shift differences between the native and random coil states and in (C) with the magnitude of the experimental shift difference between the oxidised and reduced states of nDsbD. Shift differences between the major and minor states for E69, Y71 and K73, for which the sign of the shift difference has been obtained, are compared with the predicted shift differences between the native and random states and in (D) and with the magnitude of the experimental shift difference between the reduced and oxidised states of nDsbD in (E).

however, resemble the chemical shift differences between the oxidised and reduced isoforms of nDsbD (Fig. 6C).[32] However, the correlation in Fig. 6C is not perfect; the differences between the chemical shifts of the minor state of $nDsbD_{ox}$ and those of $nDsbD_{red}$ likely reflect the local electronic and steric differences between having a disulfide bond (in the minor state of $nDsbD_{ox}$) and two cysteine thiols (in $nDsbD_{red}$) in the active site. Importantly, the sign of the chemical shift differences between the major and minor state, which could be determined experimentally for E69, Y71 and K73, further indicated that the minor state structure of the cap loop of $nDsbD_{ox}$ is not disordered (Fig. 6D) but instead may be similar to that adopted in $nDsbD_{red}$ (Fig. 6E).

Coupling between the active site and the cap loop gives rise to the alternative minor state of oxidised nDsbD

Coupling between the dynamics of active site and the cap loop also explains why $nDsbD_{ox}$ features an alternative minor state, which we detected by NMR relaxation dispersion. In the alternative minor state, the C103 and C109 side chains may adopt a 'reduced-like' conformation. Both side chains adopt a gauche- conformation ($\chi_1 \approx -60°$) in $nDsbD_{ox}$, but a trans conformation ($\chi_1 \approx 180°$) in $nDsbD_{red}$. In MD simulations of both redox states, rare excursions of one or the other χ_1, but never both, to the alternative conformation are observed. We postulate that in the minor state of $nDsbD_{ox}$, both of the cysteine side chains adopt the 'reduced-like' trans conformation ($\chi_1 \approx 180°$). In this state, the cap loop could then pack tightly onto the active-site disulfide bond, as observed in MD simulations of $nDsbD_{red}$. The backbone ^{15}N chemical shifts of this state consequently resemble those of the reduced protein. Model building of a disulfide bond into the reduced 3PFU crystal structure followed by energy minimisation with XPLOR[71] showed that the resulting 'oxidised' structure maintains the 'reduced-like' trans conformation ($\chi_1 \approx -140°$) for the cysteine side chains and the gauche- conformation for F70. This 'reduced-like' conformation for $nDsbD_{ox}$, with a more tightly packed active site and cap loop which lack frustration, might be enthalpically more

favourable and entropically less favourable than the major state of $nDsbD_{ox}$ as shown by the analysis of relaxation dispersion data collected at multiple temperatures (Fig. S4).

NMR relaxation dispersion experiments with a loop deletion mutant

We confirmed the tight coupling between the dynamics of the cap loop and the active site by NMR relaxation dispersion experiments on an nDsbD mutant. We generated an nDsbD mutant with a truncated cap loop in which the eight residues H66-K73 are replaced by A-G-G (Δloop-nDsbD). Analysis of the NMR chemical shifts and NOE patterns indicates that the deletion of the cap loop does not lead to any significant change in structure in Δloop-nDsbD. In the absence of F70, the cap loop will no longer closely pack onto the disulfide bond. No relaxation dispersion is detected in the truncated cap loop variant, as shown for W65 (Fig. 5G). For A104 (A99), a much sharper amide peak is observed in the HSQC spectrum of Δloop-$nDsbD_{ox}$ and this residue shows a flat dispersion profile (Fig. 5H). Importantly, the amide peaks for C103 and C109, which are invisible in the wild-type oxidised protein, can be detected for Δloop-$nDsbD_{ox}$. ^{15}N relaxation dispersion profiles for C103 (C98) and C109 (C104) are also flat (Fig. 5I). Thus, truncation of the cap loop alters the μs-ms dynamics of the cap-loop region and the active-site cysteines, further supporting the proposal of tight coupling between the cap loop and the active-site cysteines.

Conclusion

We have studied oxidised and reduced nDsbD using NMR experiments and microsecond duration MD simulations and have demonstrated that the conformational dynamics of the active-site cysteines and the cap loop are coupled and behave in an oxidation-state-dependent manner. We showed that the cap loop is rigid in $nDsbD_{red}$, while it exhibits more complex dynamics in $nDsbD_{ox}$ (Fig. 7). While the cap loop is predominately closed and ordered in both oxidation states, for $nDsbD_{red}$ we found no evidence for a significant population with an open cap loop. Our results argue that the cap loop of $nDsbD_{red}$ remains closed

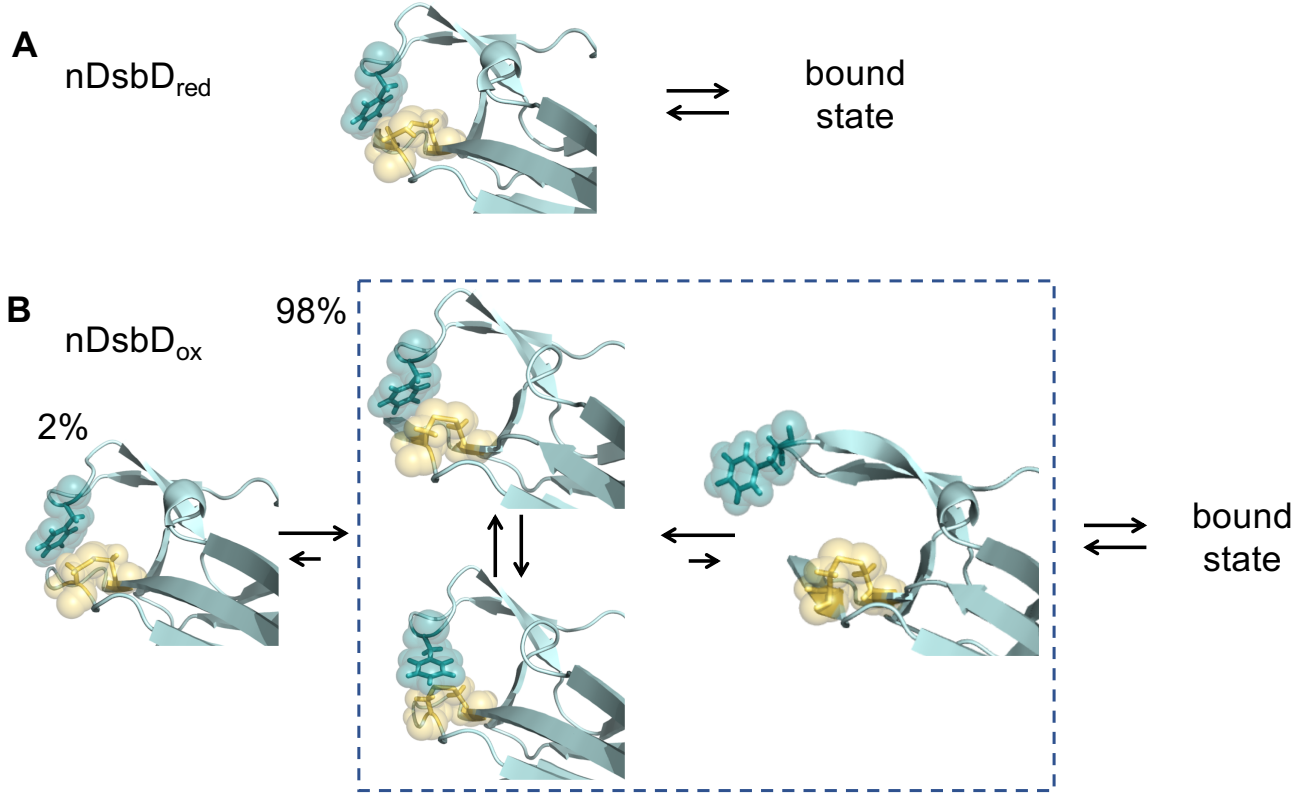

Figure 7: Local frustration in oxidised but not in reduced nDsbD. (A) The cap loop in nDsbD$_{red}$ maintains a closed conformation shielding the active site cysteine thiols. The nDsbD$_{red}$ cap loop maintains a closed conformation and may only open to expose the cysteine thiols via an induced-fit mechanism when it encounters its legitimate binding partners, CcmG, DsbC and DsbG. (B) nDsbD$_{ox}$ undergoes more complex dynamics as a result of local structural frustration. F70 interacts with the sulfur of C109 both in its gauche- (top left structure in dashed rectangle) and trans (lower left structure in dashed rectangle) orientation . These mutually competing interactions destabilise the packing of the cap loop onto the active site. Consequently, open conformations (right-hand structure in dashed rectangle) are accessible in nDsbD$_{ox}$ and these would allow nDsbD$_{ox}$ to form complexes with its legitimate binding partner, cDsbD$_{red}$, via a conformational selection mechanism. (in these three structures C103 and C109 are gauche-). The left-hand structure shows a reduced-like minor (2F70 (dark teal), C103 and C109 (yellow) are shown with sticks and a surface representation. (A) is from the 3PFU X-ray structure of nDsbD$_{red}$, the left-hand panel in (B) is the energy minimised 3PFU structure with a disulfide bond incorporated, the central and right-hand structures in (B) are 'snapshots' from the MD simulations of nDsbD$_{ox}$.

at all times, protecting the active-site cysteine thiol groups from non-cognate reactions in the oxidising environment of the periplasm of Gram-negative bacteria. The $nDsbD_{red}$ cap loop may only open to expose the cysteine thiols via an induced-fit mechanism when it encounters its legitimate binding partners, for example CcmG, DsbC and DsbG. In $nDsbD_{ox}$, on the other hand, the cap loop opens spontaneously in MD simulations and while fully open conformations of the cap loop tended to close, partially open structures were stable. Thus, $nDsbD_{ox}$ may form complexes with its legitimate binding partner, $cDsbD_{red}$, via a conformational selection mechanism. NMR relaxation dispersion experiments provided no evidence for a long-lived open or disordered conformation of the cap loop. Instead, a minor state with a 'reduced-like' conformation in the active site and cap loop is observed for $nDsbD_{ox}$.

Importantly, combining NMR experiments and MD simulations, we showed how local frustration[14,15] in $nDsbD_{ox}$, but not in $nDsbD_{red}$, gives rise to these differences in the dynamics of the two redox isoforms. Local frustration has been highlighted in the interaction interfaces of many protein complexes.[14] The mutually exclusive favourable interactions result in a dynamic equilibrium of competing structures determining which parts of a protein are flexible. In $nDsbD_{red}$, the cap loop packs perfectly onto the active-site cysteines and the closed conformation is stable. By contrast, in $nDsbD_{ox}$, the disulfide bond disrupts this close fit of the aromatic ring of F70 and consequently the side-chain of F70 switches between gauche- and trans orientations. As the phenyl ring of F70 is no longer locked in a single conformation, the cap loop is more flexible and can open. Therefore, the disulfide bond introduces local frustration in nDsbD. This means that it is the oxidation state of the cysteine pair that acts as a 'switch' controlling the presence or absence of local frustration in the nDsbD active site, that then determines the dynamic behaviour of the cap loop. Modulation of local frustration, such as that observed here for nDsbD, may play a wider role in biomolecular recognition. Ultimately, controlled introduction of frustration, mimicking natural systems such as DsbD, may serve as a novel design principle for synthetic molecular

devices.

Acknowledgement

L.S.S. acknowledges the Biotechnology and Biological Sciences Research Council (BBSRC) for a graduate studentship. D.A.I.M. acknowledges funding from an MRC Career Development Award MR/M009505/1. M.S.P.S. acknowledges funding from the Wellcome Trust (grant number 208361/Z/17/Z) and the BBSRC (grant number BB/R00126X/1). C.R. acknowledges funding from the Wellcome Trust (grant numbers 079440, 092532). We thank Prof. D. Flemming Hansen for helpful discussions. We thank Nick Soffe for help with the NMR pulse sequence programming. The authors would like to acknowledge the use of the University of Oxford Advanced Research Computing (ARC) facility in carrying out this work.

Supporting information

Supporting information includes figures illustrating the analysis of RDC data for nDsbD, analysis of fast-time scale motions in the cap loop as revealed by NMR and MD, analysis of relaxation dispersion experiments at multiple temperatures, and tables with the plasmids used in this study, RDC and 'model-free' analysis as well as a table on determination of sign for the chemical shifts of the invisible, sparsely populated state of $nDsbD_{ox}$.

References

(1) Baldwin, A. J.; Kay, L. E. *Nat. Chem. Biol.* **2009**, *5*, 808–814.

(2) Sekhar, A.; Velyvis, A.; Zoltsman, G.; Rosenzweig, R.; Bouvignies, G.; Kay, L. E. *Elife* **2018**, *7*, e32764.

(3) Lange, O. F.; Lakomek, N.-A.; Farès, C.; Schröder, G. F.; Walter, K. F. A.; Becker, S.; Meiler, J.; Grubmüller, H.; Griesinger, C.; de Groot, B. L. *Science* **2008**, *320*, 1471–1475.

(4) Sugase, K.; Dyson, H. J.; Wright, P. E. *Nature* **2007**, *447*, 1021–1025.

(5) Olsson, S.; Noé, F. *J. Am. Chem. Soc.* **2017**, *139*, 200–210.

(6) Pan, A. C.; Jacobson, D.; Yatsenko, K.; Sritharan, D.; Weinreich, T. M.; Shaw, D. E. *Proc. Natl. Acad. Sci. U. S. A.* **2019**, *116*, 4244–4249.

(7) Robustelli, P.; Stafford, K. A.; Palmer, A. G. *J. Am. Chem. Soc.* **2012**, *134*, 6365–6374.

(8) Zhang, H. L.; Hou, G. J.; Lu, M. M.; Ahn, J.; Byeon, I. J. L.; Langmead, C. J.; Perilla, J. R.; Hung, I.; Gor'kov, P. L.; Gan, Z. H.; Brey, W. W.; Case, D. A.; Schulten, K.; Gronenborn, A. M.; Polenova, T. *J. Am. Chem. Soc.* **2016**, *138*, 14066–14075.

(9) Paul, F.; Wehmeyer, C.; Abualrous, E. T.; Wu, H.; Crabtree, M. D.; Schöneberg, J.; Clarke, J.; Freund, C.; Weikl, T. R.; Noé, F. *Nat. Commun.* **2017**, *8*, 1095.

(10) Peters J. H.; de Groot, B. L. *PLoS Comput. Biol.* **2012**, *8*, e1002704.

(11) Robustelli, P.; Trbovic, N.; Friesner, R. A.; Palmer, A. G. *J. Chem. Theory Comput.* **2013**, *9*, 5190–5200.

(12) Boehr, D. D.; Nussinov, R.; Wright, P. E. *Nat. Chem. Biol.* **2009**, *5*, 789–796.

(13) Baldwin, A. J.; Knowles, T. P. J.; Tartaglia, G. G.; Fitzpatrick, A. W.; Devlin, G. L.; Shammas, S. L.; Waudby, C. A.; Mossuto, M. F.; Meehan, S.; Gras, S. L.; Christodoulou, J.; Anthony-Cahill, S. J.; Barker, P. D.; Vendruscolo, M.; Dobson, C. M. *J. Am. Chem. Soc.* **2011**, *133*, 14160–14163.

(14) Ferreiro, D. U.; Hegler, J. A.; Komives, E. A.; Wolynes, P. G. *Proc. Natl. Acad. Sci. U. S. A.* **2007**, *104*, 19819–19824.

(15) Ferreiro, D. U.; Hegler, J. A.; Komives, E. A.; Wolynes, P. G. *Proc. Natl. Acad. Sci. U. S. A.* **2011**, *108*, 3499–3503.

(16) Ferreiro, D. U.; Komives, E. A.; Wolynes, P. G. *Q. Rev. Biophys.* **2014**, *47*, 285–363.

(17) Jenik, M.; Parra, R. G.; Radusky, L. G.; Turjanski, A.; Wolynes, P. G.; Ferreiro, D. U. *Nucleic Acids Res.* **2012**, *40*, W348–W351.

(18) Danielsson, J.; Awad, W.; Saraboji, K.; Kurnik, M.; Lang, L.; Leinartaite, L.; Marklund, S. L.; Logan, D. T.; Oliveberg, M. *Proc. Natl. Acad. Sci. U. S. A.* **2013**, *110*, 3829–3834.

(19) Das, A.; Plotkin, S. S. *Proc. Natl. Acad. Sci. U. S. A.* **2013**, *110*, 3871–3876.

(20) Cho, S. H.; Collet, J. F. *Antioxid. Redox Signal.* **2013**, *18*, 1690–1698.

(21) Depuydt, M.; Leonard, S. E.; Vertommen, D.; Denoncin, K.; Morsomme, P.; Wahni, K.; Messens, J.; Carroll, K. S.; Collet, J. F. *Science* **2009**, *326*, 1109–1111.

(22) Stirnimann, C. U.; Grutter, M. G.; Glockshuber, R.; Capitani, G. *Cell. Mol. Life Sci.* **2006**, *63*, 1642–1648.

(23) Haebel, P. W.; Goldstone, D.; Katzen, F.; Beckwith, J.; Metcalf, P. *EMBO J.* **2002**, *21*, 4774–4784.

(24) Mavridou, D. A.; Saridakis, E.; Kritsiligkou, P.; Goddard, A. D.; Stevens, J. M.; Ferguson, S. J.; Redfield, C. *J. Biol. Chem.* **2011**, *286*, 24943–24956.

(25) Rozhkova, A.; Stirnimann, C. U.; Frei, P.; Grauschopf, U.; Brunisholz, R.; Grutter, M. G.; Capitani, G.; Glockshuber, R. *EMBO J.* **2004**, *23*, 1709–1719.

(26) Stirnimann, C. U.; Rozhkova, A.; Grauschopf, U.; Grutter, M. G.; Glockshuber, R.; Capitani, G. *Structure* **2005**, *13*, 985–993.

(27) Goulding, C. W.; Sawaya, M. R.; Parseghian, A.; Lim, V.; Eisenberg, D.; Missiakas, D. *Biochemistry* **2002**, *41*, 6920–6927.

(28) Quinternet, M.; Tsan, P.; Neiers, F.; Beaufils, C.; Boschi-Muller, S.; Averlant-Petit, M. C.; Branlant, G.; Cung, M. T. *Biochemistry* **2008**, *47*, 8577–8589.

(29) Rozhkova, A.; Glockshuber, R. *J. Mol. Biol.* **2007**, *367*, 1162–1170.

(30) Schmidt, B.; Ho, L.; Hogg, P. J. *Biochemistry* **2006**, *45*, 7429–7433.

(31) Zhou, B. F.; Baldus, I. B.; Li, W. J.; Edwards, S. A.; Grater, F. *Biophys. J.* **2014**, *107*, 672–681.

(32) Mavridou, D. A.; Stelzl, L. S.; Ferguson, S. J.; Redfield, C. *Biomol. NMR Assignments* **2012**, *6*, 163–167.

(33) Mavridou, D. A.; Stevens, J. M.; Goddard, A. D.; Willis, A. C.; Ferguson, S. J.; Redfield, C. *J. Biol. Chem.* **2009**, *284*, 3219–3226.

(34) Mavridou, D. A.; Stevens, J. M.; Ferguson, S. J.; Redfield, C. *J. Mol. Biol.* **2007**, *370*, 643–658.

(35) Delaglio, F.; Grzesiek, S.; Vuister, G. W.; Zhu, G.; Pfeifer, J.; Bax, A. *J. Biomol. NMR* **1995**, *6*, 277–293.

(36) Skinner, S. P.; Fogh, R. H.; Boucher, W.; Ragan, T. J.; Mureddu, L. G.; Vuister, G. W. *J. Biomol. NMR* **2016**, *66*, 111–124.

(37) Vranken, W. F.; Boucher, W.; Stevens, T. J.; Fogh, R. H.; Pajon, A.; Llinas, M.; Ulrich, E. L.; Markley, J. L.; Ionides, J.; Laue, E. D. *Proteins* **2005**, *59*, 687–696.

(38) Ottiger, M.; Delaglio, F.; Bax, A. *J. Magn. Reson.* **1998**, *131*, 373–378.

(39) Ottiger, M.; Tjandra, N.; Bax, A. *J. Am. Chem. Soc.* **1997**, *119*, 9825–9830.

(40) Boyd, J.; Hommel, U.; Campbell, I. D. *Chem. Phys. Lett.* **1990**, *175*, 477–482.

(41) Kay, L. E.; Torchia, D. A.; Bax, A. *Biochemistry* **1989**, *28*, 8972–8979.

(42) Palmer, A. G.; Skelton, N. J.; Chazin, W. J.; Wright, P. E.; Rance, M. *Mol. Phys.* **1992**, *75*, 699–711.

(43) Smith, L. J.; Bowen, A. M.; Di Paolo, A.; Matagne, A.; Redfield, C. *ChemBioChem* **2013**, *14*, 1780–1788.

(44) Lipari, G.; Szabo, A. *J. Am. Chem. Soc.* **1982**, *104*, 4546–4559.

(45) Lipari, G.; Szabo, A. *J. Am. Chem. Soc.* **1982**, *104*, 4559–4570.

(46) Abragam, A. *The principles of nuclear magnetism*; The International series of monographs on physics; Clarendon Press: Oxford,, 1961.

(47) Boyd, J.; Redfield, C. *J. Am. Chem. Soc.* **1998**, *120*, 9692–9693.

(48) Mandel, A. M.; Akke, M.; Palmer, A. G. *J. Mol. Biol.* **1995**, *246*, 144–163.

(49) Loria, J. P.; Rance, M.; Palmer, A. G. *J. Am. Chem. Soc.* **1999**, *121*, 2331–2332.

(50) Mulder, F. A. A.; Skrynnikov, N. R.; Hon, B.; Dahlquist, F. W.; Kay, L. E. *J. Am. Chem. Soc.* **2001**, *123*, 967–975.

(51) Vallurupalli, P.; Hansen, D. F.; Kay, L. E. *Proc. Natl. Acad. Sci. U. S. A.* **2008**, *105*, 11766.

(52) Baldwin, A. J.; Hilton, G. R.; Lioe, H.; Bagnéris, C.; Benesch, J. L.; Kay, L. E. *J. Mol. Biol.* **2011**, *413*, 310 – 320.

(53) Alderson, T. R.; Roche, J.; Gastall, H. Y.; Dias, D. M.; Pritišanac, I.; Ying, J.; Bax, A.; Benesch, J. L. P.; Baldwin, A. J. *Nat. Commun.* **2019**, *10*, 1068.

(54) Skrynnikov, N. R.; Dahlquist, F. W.; Kay, L. E. *J. Am. Chem. Soc.* **2002**, *124*, 12352–12360.

(55) Van Der Spoel, D.; Lindahl, E.; Hess, B.; Groenhof, G.; Mark, A. E.; Berendsen, H. J. C. *J. Comput. Chem.* **2005**, *26*, 1701–1718.

(56) Hekkelman, M. L.; Beek, T. A. H. T.; Pettifer, S. R.; Thorne, D.; Attwood, T. K.; Vriend, G. *Nucleic Acids Res.* **2010**, *38*, W719–W723.

(57) MacKerell, A. D. et al. *J. Phys. Chem. B* **1998**, *102*, 3586–3616.

(58) Mackerell, A. D.; Feig, M.; Brooks, C. L. *J. Comput. Chem.* **2004**, *25*, 1400–1415.

(59) Essmann, U.; Perera, L.; Berkowitz, M. L.; Darden, T.; Lee, H.; Pedersen, L. G. *J. Chem. Phys.* **1995**, *103*, 8577–8593.

(60) Bjelkmar, P.; Larsson, P.; Cuendet, M. A.; Hess, B.; Lindahl, E. *J. Chem. Theory Comput.* **2010**, *6*, 459–466.

(61) Hess, B. *J. Chem. Theory Comput.* **2008**, *4*, 116–122.

(62) Bussi, G.; Donadio, D.; Parrinello, M. *J. Chem. Phys.* **2007**, *126*.

(63) Parrinello, M.; Rahman, A. *J. Appl. Phys.* **1981**, *52*, 7182–7190.

(64) Chandrasekhar, I.; Clore, G. M.; Szabo, A.; Gronenborn, A. M.; Brooks, B. R. *J. Mol. Biol.* **1992**, *226*, 239–250.

(65) Shen, Y.; Bax, A. *J. Biomol. NMR* **2013**, *56*, 227–241.

(66) Salonen, L. M.; Ellermann, M.; Diederich, F. *Angew. Chem., Int. Ed.* **2011**, *50*, 4808–4842.

(67) Grey, M. J.; Wang, C. Y.; Palmer, A. G. *J. Am. Chem. Soc.* **2003**, *125*, 14324–14335.

(68) Shaw, D. E.; Maragakis, P.; Lindorff-Larsen, K.; Piana, S.; Dror, R. O.; Eastwood, M. P.; Bank, J. A.; Jumper, J. M.; Salmon, J. K.; Shan, Y. B.; Wriggers, W. *Science* **2010**, *330*, 341–346.

(69) Xue, Y.; Ward, J. M.; Yuwen, T. R.; Podkorytov, I. S.; Skrynnikov, N. R. *J. Am. Chem. Soc.* **2012**, *134*, 2555–2562.

(70) Dill, K. A.; Bromberg, S. *Molecular Driving Forces: Statistical Thermodynamics in Biology, Chemistry, Physics and Nanoscience*; Garland Science: New York, 2010.

(71) Brunger, A. T. *X-PLOR Version 3.1: A system for X-ray crystallography and NMR*; Yale University Press: New Haven CT, 1992.

SUPPORTING INFORMATION

Local frustration determines loop opening in protein-protein association

Lukas S. Stelzl,[†,¶] Despoina A.I. Mavridou,[†,§] Andrew J. Baldwin,[‡] Stuart J. Ferguson,[†] Mark S. P. Sansom,[*,†] and Christina Redfield[*,†]

[†]Department of Biochemistry, University of Oxford, South Parks Road, Oxford OX1 3QU, U.K.

[‡]Department of Chemistry, Physical and Theoretical Chemistry Laboratory, University of Oxford, South Parks Road, Oxford OX1 3QZ, U.K.

[¶] Current address: Department of Theoretical Biophysics, Max Planck Institute of Biophysics, Max-von-Laue Str. 3, 60438 Frankfurt, Germany

[§] Current address: MRC Centre for Molecular Bacteriology and Infection, Department of Life Sciences, Imperial College London, Kensington, London, SW7 2DD, U.K.

[*]Corresponding authors –

C.R. email: christina.redfield@bioch.ox.ac.uk

M.S.P.S. email: mark.sansom@bioch.ox.ac.uk

This PDF file includes:

Supporting Figures S1 to S4
Tables S1 to S4
Supporting Information reference citations

SUPPORTING FIGURES

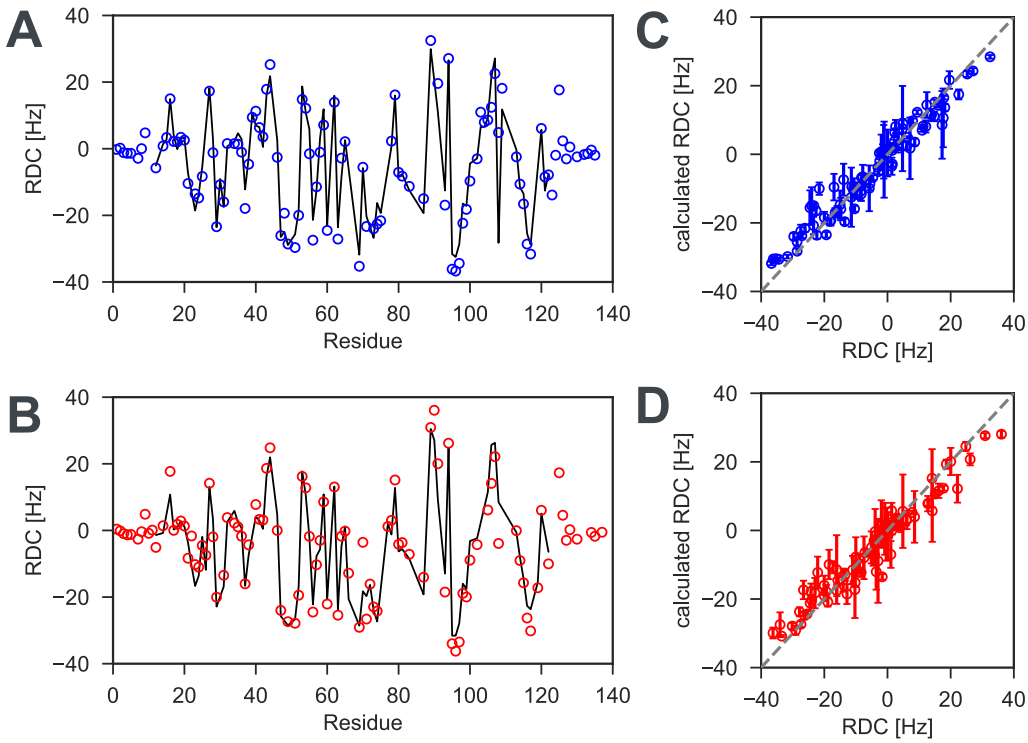

Figure S1: ^{1}H -^{15}N Residual dipolar couplings (RDCs) for (A) reduced and (B) oxidised nDsbD. To probe the solution structure of oxidised and reduced nDsbD, ^{1}H-^{15}N residual RDCs, which are sensitive reporters of protein structure, were measured. Experimental RDCs are indicated by the open circles while RDCs calculated by fitting the alignment tensor to the X-ray structure (PDB:3PFU for reduced and PDB:1L6P for oxidised nDsbD) are indicated by the solid line. For most residues very similar RDCs were measured for reduced and oxidised nDsbD. The small RDCs measured for residues 1-8 and 126-135 in both redox states are likely to indicate conformational dynamics leading to averaging of these RDCs; values for most of these residues cannot be predicted from the X-ray structures because electron density is not observed before residue 8 and after residue 125 in the structures. By contrast, the RDCs for the core β-sandwich are predicted very well by the X-ray structures; Q values of 0.21 and 0.17 are obtained for oxidised and reduced nDsbD, respectively (Table S2). When fits are carried out for residues 12-122, which includes the core β-sandwich and the active-site/cap-loop residues, Q values of 0.24 and 0.19 are obtained for oxidised and reduced nDsbD, respectively (Table S2). The similar Q values for the two sets of RDCs suggest that the orientation of the active-site/cap-loop residues relative to the core β-sandwich of both oxidised and reduced nDsbD in solution is well-described by the X-ray structures in which the cap loop adopts a closed conformation. Experimental RDCs are compared with RDCs calculated from MD simulations for (C) reduced and (D) oxidised nDsbD. For both $nDsbD_{red}$ and $nDsbD_{ox}$, the agreement between calculated and experimental RDCs improved for the 1μs MD ensemble compared to the static X-ray structures. It is also interesting to note that the RDCs for residues 106 and 108, which gave poor agreement in the fits to the static X-ray structures due to crystal contacts, agree well with the values predicted from the MD simulations.

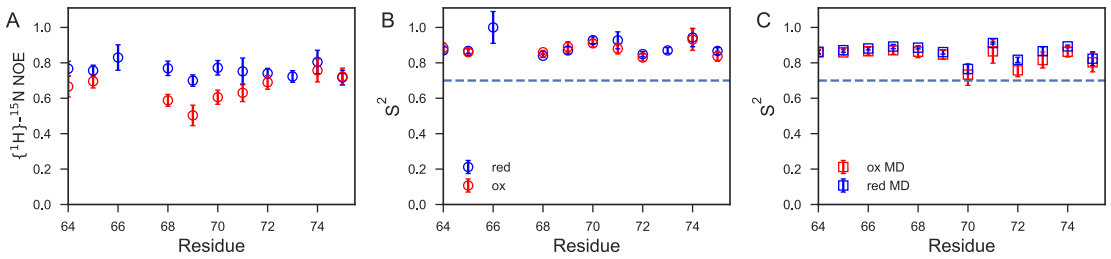

Figure S2: Fast time-scale dynamics of the cap loop. (A) Comparison of experimental $\{^1H\}$-^{15}N heteronuclear NOE values for reduced (blue) and oxidised (red) nDsbD. (B) Comparison of order parameters (S^2) derived from model-free analysis of ^{15}N relaxation data for reduced (blue) and oxidised (red) nDsbD. (C) Comparison of order parameters (S^2) derived from the MD simulations for reduced (blue) and oxidised (red) nDsbD.

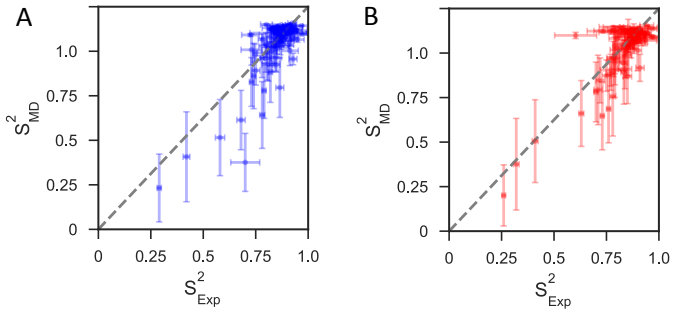

Figure S3: Comparison of backbone order parameters (S^2) derived from experimental ^{15}N relaxation data and calculated from the 1μs MD simulations for (A) reduced and (B) oxisised nDsbD. The extent of the fast-time scale (ps-ns) dynamics observed experimentally by NMR is on the whole correctly reproduced by the MD simulations. The root mean-square deviation (RMSD) between the order parameters detemined from model-free analysis and from the simulations is 0.08 for both reduced and oxidised nDsbD. The N- and C-termini were very flexible, but most residues in the folded segments of nDsbD were well ordered with $S^2 > 0.80$, which agrees with experiment.

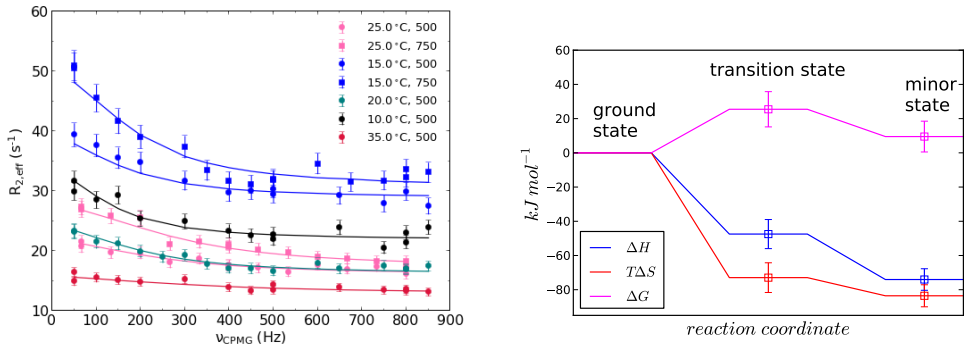

(a) (b)

Figure S4: **Analysis of the relaxation dispersion experiments at multiple temperatures.** Relaxation dispersion curves measured at 10 °C, 15 °C, 20 °C, 35 °C for W65 of oxidised nDsbD at 500 and 750 MHz and the curves from the global fitting are shown in (A). The fits at five different temperatures yield a description of the free energy landscape of the exchange process shown in (B). The minor state of oxidised nDsbD is enthalpically more favourable than the ground state. This agrees with visual inspection of the curves in (A) and the conclusion from comparing the fits obtained at 15 °C and 25 °C. The minor state is entropically less favourable than the ground state and overall it is about 10 kJ mol^{-1} less favourable (B). The fitting of the experimental curves at the five temperatures also reports on the barrier between the two states. The transition state appears to be more enthalphically favourable than the ground state. There is, however, a sizeable free energy barrier as the transition state is lower in entropy than the ground state. Note that $\Delta S^{\ddagger}$ and hence $\Delta G^{\ddagger}$ depend on the transmission coefficient κ that is used in eqn. 1.

$$k = \kappa(\frac{k_B T}{h})e^{-\Delta H^{\ddagger}/(k_B T)}e^{\Delta S^{\ddagger}/k_B} \quad (1)$$

$\Delta H^{\ddagger}$ and $\Delta S^{\ddagger}$ are the activation enthalpy and the activation entropy for the reaction. The transmission coefficient κ was set to 1.4 x 10^{-7} s^{-1} K^{-1}, the default value in CATIA [Hansen, D.F. CATIA (Cpmg, Anti-trosy, and Trosy Intelligent Analysis) 2008; http://www.biochem.ucl.ac.uk/hansen/catia/] and similar to κ 1.6 x 10^{-7} s^{-1} K^{-1} used in a previous relaxation dispersion study [1]. However, the absence of a significant enthalphic barrier was already suggested by comparing the reaction rates obtained at 15 °C and 25 °C, when fitting data at only a single temperature. There is no obvious rate increase in going from 15 °C, with k_A = 40 s^{-1}, and 25 °C, with k_A = 30 s^{-1}.

SUPPORTING TABLES

Table S1. Plasmids used in this study

Name	Description	Source
pDzn3	N-terminal domain (L2-V132) of *E. coli* DsbD (nDsbD) with a thrombin-cleavable C-terminal polyhistidine tag, Amp^R	[2-3]
pDzn8	pDzN3 with residues H66-K73 replaced by AGG	This study

Table S2 Quality factors (Q) and alignment tensor parameters (D_a, R, θ, ϕ, ψ) obtained from fits of experimental RDCs to X-ray structures for oxidised (1L6P) and reduced (3PFU) nDsbD and from analysis of the 1μs MD trajectories for oxidised and reduced nDsbD.

$nDsbD_{ox}$ using the 1L6P X-ray structure							
Region for which RDCs were fitted	**Number of residues fitted**	**Q**	**D_a**	**R**	**θ**	**ϕ**	**ψ**
8-122	87	0.34	-15.7	0.56	83.6	86.5	70.2
12-122	83	0.26	-16.4	0.61	83.1	85.1	71.0
12-122 w/o 106/108*	81	0.24	-16.8	0.61	83.7	84.8	71.7
core	46	0.21	-17.7	0.61	84.7	83.2	72.9
active site	14	0.15	-15.7	0.56	80.6	88.6	67.2
1 μs MD simulation of $nDsbD_{ox}$							
8-122	87	0.26					
$nDsbD_{red}$ using the 3PFU X-ray structure							
8-125	90	0.38	-15.2	0.56	85.2	88.8	105.3
12-122	87	0.29	-16.5	0.57	85.5	91.1	105.5
12-122 w/o 106/108*	85	0.19	-17.5	0.57	85.2	92.3	106.3
core	46	0.17	-17.5	0.61	85.0	91.7	108.6
active site	16	0.16	-18.6	0.52	88.4	93.9	106.2
1 μs MD simulation of $nDsbD_{red}$							
8-125	90	0.23					

*106/108 were excluded due to crystal contacts in the X-ray structures which may distort conformation leading to poor fits; core means α1, β-sandwich and tight turn(s); active site means α2, β-strands but not loop (69-71).

Table S3 Model-free analysis of ^{15}N relaxation data for the cap loop and the flanking β-strands.

	nDsbD$_{ox}$			**nDsbD$_{red}$**		
	{^{1}H}-^{15}N NOE	**S^2**	**τ_e (ps)**	**{^{1}H}-^{15}N NOE**	**S^2**	**τ_e (ps)**
V64	0.67	0.87	83 +/- 62	0.77	0.87	
W65	0.70	0.86	54 +/- 20	0.76	0.87	
H66				0.83	1.0	
E67						
D68	0.59	0.86	108 +/- 85	0.77	0.85	
E69	0.50	0.89	334 +/- 121	0.70	0.87	63 +/- 18
F70	0.61	0.91	246 +/- 136	0.77	0.93	
Y71	0.63	0.88	99 +/- 61	0.75	0.93	
G72	0.69	0.83	47 +/- 14	0.74	0.85	
K73				0.72		
S74	0.76	0.93		0.80	0.94	
E75	0.72	0.84		0.72	0.87	
I76	0.84	0.81				
Y77	0.78	0.82		0.87	0.86	

Table S4 ^{15}N chemical shifts in HSQC and HMQC experiments collected at 750 MHz. The sign information could be extracted with confidence for E69, Y71 and K73.

	HSQC	**HMQC**	$\Omega_{Nexp.}$(ppm)	Sign Ω_N.(Hz)
A64	117.491	117.495	-0.004	0.30 [+*ve*]
W65	122.508	122.506	+0.002	-0.15 [-*ve*]
E69	118.900	118.931	-0.031	2.36 +*ve*
F70	120.811	120.810	+0.001	-0.08 [−*ve*]
Y71	116.268	116.273	-0.005	0.38 +*ve*
K73	126.896	126.873	+0.023	-1.75 −*ve*

For E69 and K73 $|\Omega_N|$, is found to be > 0.3Hz, while for Y71 $|\Omega_N|$ is close to the cut-off value of 0.3 Hz proposed by Skrynnikov *et al.* for confidently reconstructing the sign information [4]. The positive Ω_N for E69 and Y71 shows that their minor state peaks are upfield of the major state peaks. The minor state peaks are at lower ppm value than the major state resonances. Similarly, the peaks for E69 and Y71 in reduced nDsbD have smaller ^{15}N chemical shift than in the oxidised protein. For K73, a negative Ω_N was found, and thus the minor state peak for K73 has larger ppm value than in the major state.

References

1. Choy, W. Y.; Zhou, Z.; Bai, Y. W.; Kay, L. E., An N-15 NMR spin relaxation dispersion study of the folding of a pair of engineered mutants of apocytochrome b(562). *J Am Chem Soc* **2005,** *127* (14), 5066-5072.
2. Mavridou, D. A.; Stevens, J. M.; Goddard, A. D.; Willis, A. C.; Ferguson, S. J.; Redfield, C., Control of periplasmic interdomain thiol:disulfide exchange in the transmembrane oxidoreductase DsbD. *J Biol Chem* **2009,** *284* (5), 3219-26.
3. Mavridou, D. A.; Stelzl, L. S.; Ferguson, S. J.; Redfield, C., ^{1}H, ^{13}C and ^{15}N resonance assignments for the oxidized and reduced states of the N-terminal domain of DsbD from *Escherichia coli*. *Biomol NMR Assign* **2012,** *6* (2), 163-7.
4. Skrynnikov, N. R.; Dahlquist, F. W.; Kay, L. E., Reconstructing NMR spectra of "invisible" excited protein states using HSQC and HMQC experiments. *J Am Chem Soc* **2002,** *124* (41), 12352-12360.